Journal of Alloys and Compounds 614 (2014) 271–276

Contents lists available at ScienceDirect

Journal of Alloys and Compounds

journal homepage: www.elsevier.com/locate/jalcom

Solvothermal synthesis and electrochemical performance of Li_2MnSiO_4/C cathode materials for lithium ion batteries

Yan-Chao Wang [a,b], Shi-Xi Zhao [a,*], Peng-Yuan Zhai [a,b], Fang Li [a], Ce-Wen Nan [b]

[a] Graduate School at Shenzhen, Tsinghua University, Shenzhen 518055, China
[b] School of Materials Science and Engineering, Tsinghua University, Beijing 100084, China

ARTICLE INFO

Article history:
Received 15 February 2014
Received in revised form 15 June 2014
Accepted 16 June 2014
Available online 24 June 2014

Keywords:
Cathode material
Li_2MnSiO_4
Solvothermal synthesis
Carbon coating
Ni-modified

ABSTRACT

Orthorhombic structure Li_2MnSiO_4/C with *Pmn2₁* space group is synthesized by the solvothermal method. Carbon coating and Ni^{2+} doping are used to improve the electronic conductivity and the cycling performance of Li_2MnSiO_4 cathode material, respectively. The particles of Li_2MnSiO_4/C are much smaller and more uniform than those of Li_2MnSiO_4 due to the carbon coating. It is shown that Ni^{2+} has been reduced into metal Ni during the synthesis process. The synthesized Ni-modified Li_2MnSiO_4/C (denoted as (LMS@Ni)/C) cathode material exhibits better electrochemical performance in comparison with Li_2MnSiO_4/C, attributing to higher lithium ion diffusion coefficient as well as electronic conductivity. The initial discharge capacity of (LMS@Ni)/C is 274.5 mA h g^{-1} and the reversible capacity after 20 cycles is 119.8 mA h g^{-1} at 25 °C.

1. Introduction

Lithium ion batteries are widely applied in energy storage and conversion. The expanded applications of Lithium ion batteries in automobiles, aerospace, and power-grid demand the long-life and light-weight batteries, which largely depend on the choice of cathode materials [1–3]. $(XO_4)_n^-$ polyanion compounds have attracted lots of attention for their unique properties as cathode materials [4–6]. Of these materials, the olivine lithium iron phosphate ($LiFePO_4$) has been widely studied due to its excellent structure stability, as well as inexpensive and environmental benign characteristics [6,7]. Despite these advantages, it suffers from the low electronic conductivity. To solve this issue, numerous strategies have been utilized, including cationic doping, carbon coating and nanoparticle synthesizing [6,8–10]. Nevertheless, the energy density of $LiFePO_4$ is relatively limited partially due to only one lithium ion extraction from the host. Following the successful development of $LiFePO_4$ cathode, lithium transition metal silicates (Li_2MSiO_4, M = Fe, Mn, Co, Ni) are regarded as materials of considerable potential because of their high theoretical capacity (>300 mA h g^{-1}) [5,11–14]. And a reversible capacity of 333 mA h g^{-1} can be demonstrated because two lithium ions can be extracted from Li_2MnSiO_4, corresponding to Mn^{2+}/Mn^{3+} and Mn^{3+}/Mn^{4+} [12].

However, Li_2MnSiO_4 as a cathode material for practical applications still have several issues to be solved [15–19]. First, it is difficult to obtain a phase-pure sample, some inactive impurity phases such as MnO and Li_2SiO_3 always appear in the resultant. Second, its low electronic conductivity ($\sim 10^{-14}$ S cm^{-1}) and low lithium diffusion coefficient ($\sim 10^{-16}$ cm^2 S^{-1}) severely limit the rate performance. Furthermore, its structural instability caused by delithiation and Mn dissolution leads to capacity rapidly fading during the cycling process. Therefore, Li_2MnSiO_4 materials generally exhibit poor practical electrochemical performance. Effective strategies to improve the electrochemical performance of Li_2MnSiO_4 include carbon coating, doping with other cations to partially replace Mn^{2+}, and decreasing the particle size [20–23]. It has been demonstrated that decreasing the particle size can shorten the pathway for Li^+ transfer, which will weaken the negative effect of low Li^+ diffusion coefficient [20,24].

In recent years, various methods have been used to prepare Li_2MnSiO_4 materials, such as solid-state reaction, polyol method, and sol–gel process [25–28]. In order to obtain samples with nano particle size and high surface area, the solvothermal method was used to prepare Li_2MnSiO_4 with carbon coating in this study. To further improve the cycling performance of Li_2MnSiO_4/C, we intended to substitute Ni^{2+} for Mn^{2+} in Li_2MnSiO_4 to improve its structural stability. The effect of carbon coating and Ni^{2+} doping on the structure, morphology and electrochemical performance of Li_2MnSiO_4 was investigated.

* Corresponding author. Tel./fax: +86 0755 26036372.
E-mail address: zhaosx@sz.tsinghua.edu.cn (S.-X. Zhao).

http://dx.doi.org/10.1016/j.jallcom.2014.06.086
0925-8388/

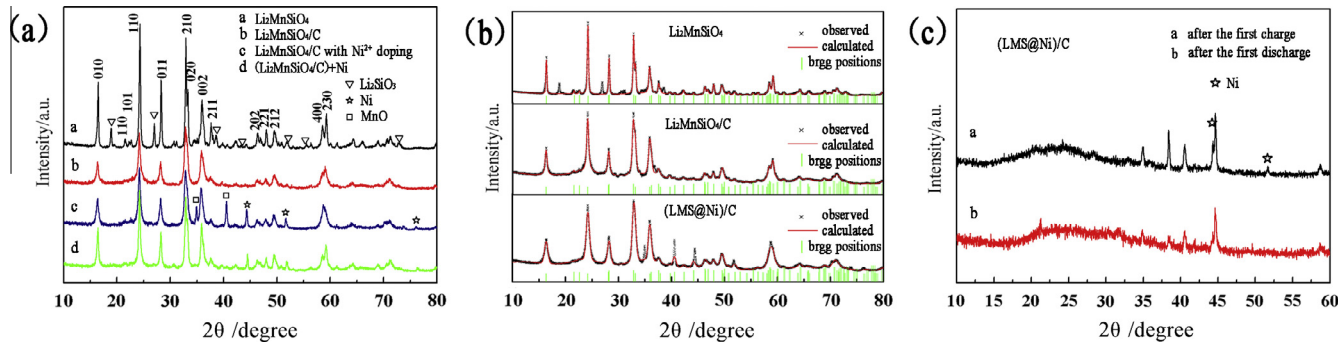

Fig. 1. XRD patterns of all samples.

Table 1
Lattice parameters of the Li_2MnSiO_4, Li_2MnSiO_4/C and (LMS@Ni)/C nanocomposites.

	a (Å)	*b* (Å)	c (Å)	Rwp (%)	Rp (%)
Li_2MnSiO_4	6.296(8)	5.377(7)	4.990(7)	19.98	13.12
Li_2MnSiO_4/C	6.298(9)	5.377(0)	4.984(3)	7.78	5.56
(LMS@Ni)/C	6.291(3)	5.380(7)	4.980(6)	10.92	7.50

2. Experimental

2.1. Preparation

Li_2MnSiO_4/C with Ni^{2+} doping was prepared via the solvothermal method by using starch as the carbon source. Firstly, $C_{19}H_{42}BrN$ (0.1 mmol, Aladdin, 99%) was dissolved in methanol (45 ml). Secondly, $C_2H_3O_2Li{\cdot}2H_2O$ (Aladdin, 99%), $MnC_4H_6O_4{\cdot}4H_2O$ (Aladdin, 99%), Si $(OC_2H_5)_4$ (Aladdin, 99%) and $NiC_4H_6O_4{\cdot}4H_2O$ (Aladdin, 99%) were added into the above solution with the molar ratio of 2.2:0.95:1:0.05. Finally, glacial acetic acid (1.5 mL) was added as a catalyst. After stirring for 6 h, the homogeneous solution was loaded into a 100 ml Teflon-lined autoclave and maintained at 120 °C for 20 h. The jelly-like product was dried at 60 °C 12 h in a vacuum. The obtained precursor was thoroughly ground and mixed with starch suspension with a weight ratio of Li_2MnSiO_4:C of 2:1. After stirring at 40 °C for 5 h, the mixture was dried at 60 °C for 12 h. The dried product was heat treated at 450 °C for 2 h and then 700 °C for 10 h in Ar (95%)/H_2 (5%) atmosphere to obtain Li_2MnSiO_4 with carbon coating and Ni^{2+} doping.

Similar processes were used to prepare Li_2MnSiO_4 and Li_2MnSiO_4/C materials with a molar ratio of Li^+:Mn^{2+}:SiO_4^{4-} of 2.2:1:1.

2.2. Physical characterization

X-ray diffraction (XRD, D/MAX-2500, Rigaku, Japan, Cu Kα radiation, 40 kV, 100 mA), scanning electron microscope (SEM, S-4800, Hitachi, Japan, 5.0 kV), and transmission electron microscope (TEM, JEM-2011, JEOL, Japan, 200 kV) were used to characterize the structure and the morphology of the prepared samples. The content of carbon was measured by thermogravimetry analysis (TG, STA 449 F3, Jupiter) for the Li_2MnSiO_4/C nanocomposite. The specific surface area of each cathode materials (denoted by $a_{s,BET}$) was obtained by analysis of nitrogen adsorption–desorption isotherms recorded at 77 K on an adsorption analyzer (Belsorp-mini, BEL, Japan).

2.3. Electrochemical measurements

The electrochemical performance of as-prepared samples was characterized with coin-type cells (CR2032). The cathode was fabricated by mixing active material, acetylene black, and polyvinylidene fluoride with a weight ratio of 80:10:10 in *N*-methyl pyrrolidone (NMP) to form homogenous slurry. The slurry was then pasted on an Al foil current collector, and the coated film was dried at 120 °C for 8 h. The resulting film was pressed, punched into circular discs with a diameter of 15 mm, and the thickness of the cathode material was about 120 μm with an average loading of 1.6–2.8 mg cm^{-2}. The electrolyte was $LiPF_6$ (1M) in ethylene carbonate and dimethyl carbonate (1:1 *v*/*v*). All the cells were assembled in an argon-filled glove box with O_2 and H_2O levels below 2 ppm with lithium metal as the anode. Electrochemical measurements were carried out using a battery test system (C2001A, Land, China) in a voltage range of 1.5–4.8 V at 0.05 C (1 C = 333 mA g^{-1}). The specific capacity of each sample was calculated based on the mass of Li_2MnSiO_4, excluding the amount of carbon coating. Electrochemical impedance spectroscopy (EIS) was measured on an electrochemical workstation (CHI660D, Chenhua, China) in the frequency range from 1 mHz to 100 kHz.

3. Results and discussion

3.1. XRD, SEM, TEM and TG analysis

The powder XRD patterns of the as-prepared Li_2MnSiO_4, Li_2MnSiO_4/C, and Li_2MnSiO_4/C with Ni^{2+} doping are shown in Fig. 1(a). All diffraction patterns can be indexed to the orthorhombic structure with a *Pmn2₁* space group [29], and the broad diffraction peaks indicate the synthesized samples with low degree of crystallization. In addition, there are some impurity phases in the resultants (labeled in Fig. 1(a)) such as Li_2SiO_3 in Li_2MnSiO_4 and MnO in Li_2MnSiO_4/C with Ni^{2+} doping. These impurities have also been reported previously [16,28–31]. No impurity is observed in the diffraction pattern of Li_2MnSiO_4/C sample, indicating that the carbon coating can inhibit the formation of impurity phases. In the diffraction pattern of Ni^{2+} doped sample, some characteristic peaks of metal Ni are observed. This indicates that no Ni^{2+} ions enter into the lattice. In order to confirm the presence of metal Ni, the (Li_2MnSiO_4/C)+Ni nanocomposite as a reference sample

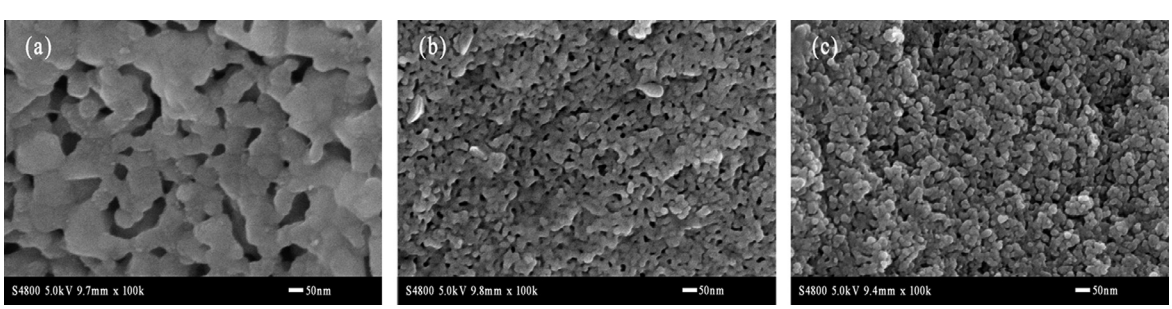

Fig. 2. SEM images of (a) Li_2MnSiO_4, (b) Li_2MnSiO_4/C and (c) (LMS@Ni)/C.

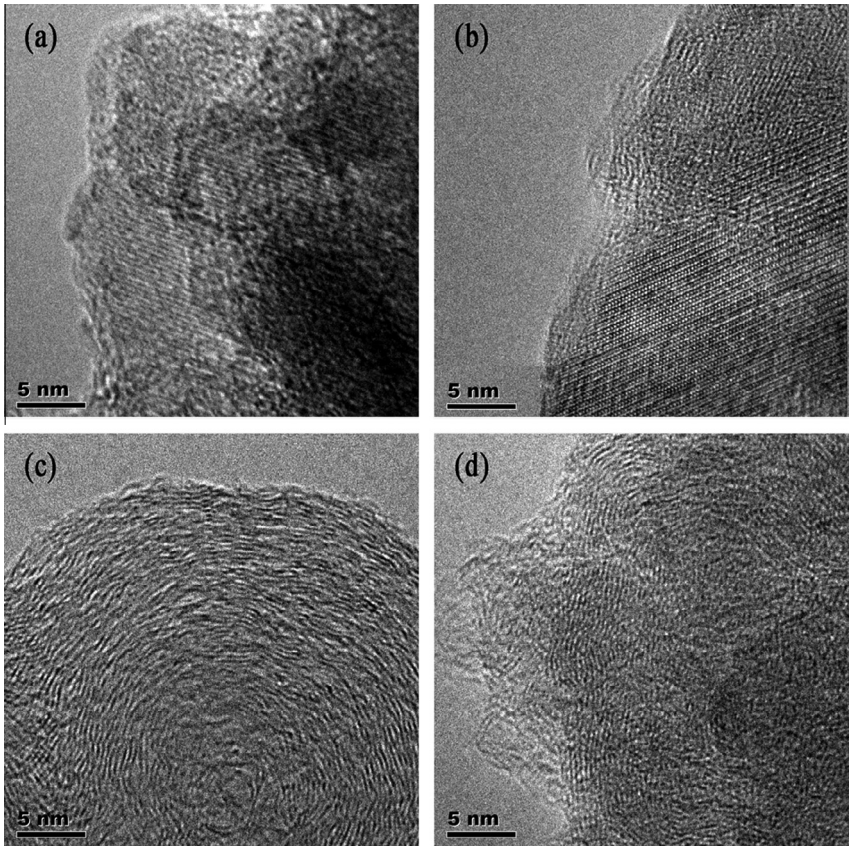

Fig. 3. TEM images of (a) Li_2MnSiO_4/C and (b) (LMS@Ni)/C before the first cycle, and for (c) Li_2MnSiO_4/C and (d) (LMS@Ni)/C after the first cycle.

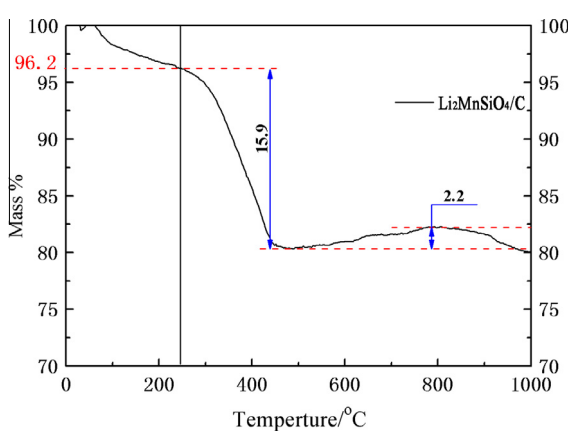

Fig. 4. TG analysis of Li_2MnSiO_4/C heated from room temperature to 1000 °C in air.

was prepared by mixing the obtained Li_2MnSiO_4/C material with Ni powders with a molar ratio of 1:0.05. It is shown that the diffraction peaks of Ni^{2+} doped sample are same with the characteristic peaks of pure Ni in reference sample, confirming that Ni^{2+} has been reduced to Ni in the Li_2MnSiO_4/C with Ni^{2+} doping sample. It was found that the reduction of Ni^{2+} was caused by the reducing atmosphere ($Ar_2 + H_2$) and carbon source during the synthesis process. Then the synthesis of Ni-modified Li_2MnSiO_4/C (denoted as (LMS@Ni)/C) nanocomposite was repeated by the solvothermal method with a molar ratio of Li^+:Mn^{2+}: SiO_4^{4-}:Ni^{2+} of 2.2:1:1:0.05 to study the effect of Ni on Li_2MnSiO_4/C. The result of XRD is identical with above.

Table 2
Carbon content of Li_2MnSiO_4/C.

Samples	Theoretical value (wt.%)	Measurements (wt.%)	The loss amount (wt.%)	Error values (wt.%)
Li_2MnSiO_4/C	33.3	15.9/96.2 = 16.5	16.8	2.2

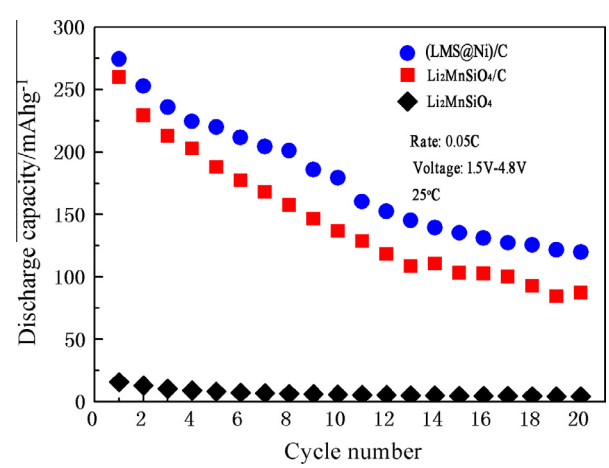

Fig. 5. Cycling performance of Li_2MnSiO_4, Li_2MnSiO_4/C and (LMS@Ni)/C.

Fig. 1(b) presents the Rietveld plots of Li_2MnSiO_4, Li_2MnSiO_4/C and (LMS@Ni)/C. The calculated lattice parameters are listed in Table 1. The unit cell parameters of Li_2MnSiO_4/C and (LMS@Ni)/C are almost identical, indicating that Ni does not occupy the lattice

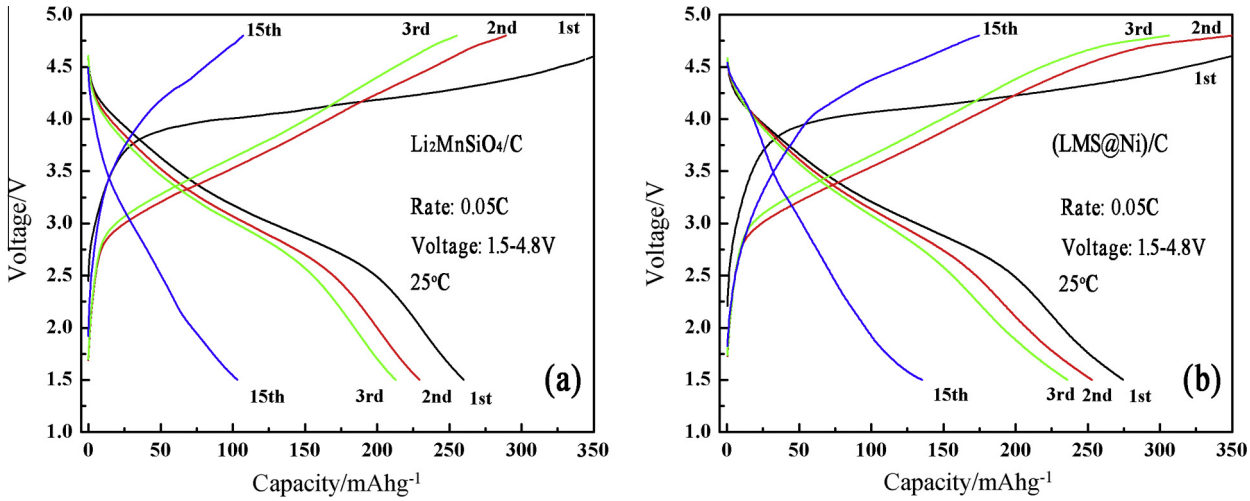

Fig. 6. Charge/discharge profiles of (a) Li_2MnSiO_4/C and (b) (LMS@Ni)/C nanocomposites.

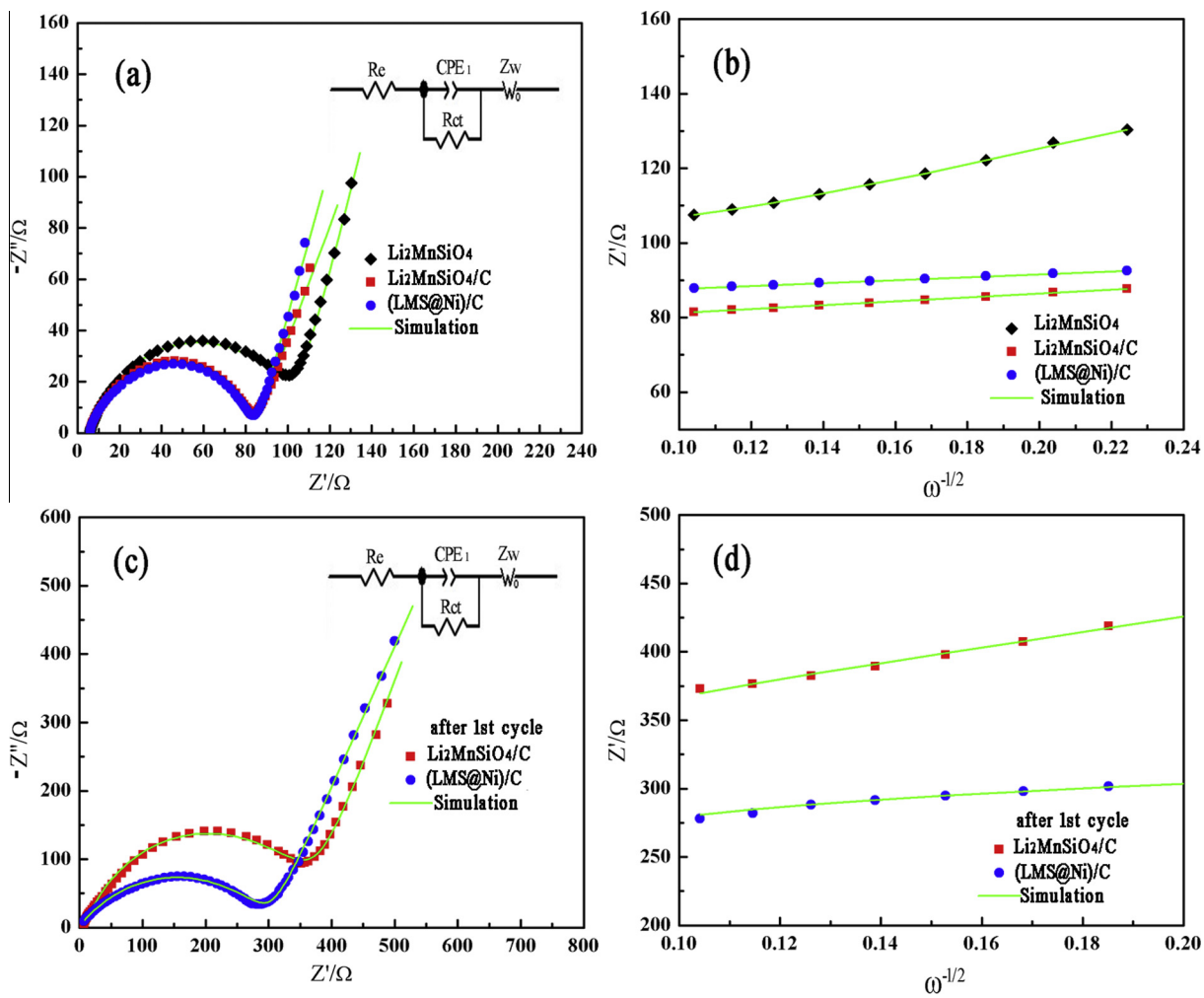

Fig. 7. (a) Nyquist plots of the Li_2MnSiO_4, Li_2MnSiO_4/C and (LMS@Ni)/C nanocomposite electrodes before cycling. (b) Linear relationship between Z' and $\omega^{-1/2}$ in the low frequency region. (c) Nyquist plots of the Li_2MnSiO_4/C and (LMS@Ni)/C nanocomposite electrodes after the first charge/discharge cycle. (d) Linear relationship between Z' and $\omega^{-1/2}$ in the low-frequency region.

of Li_2MnSiO_4/C. As a result, it is found that a straight substitution Ni^{2+} for Mn^{2+} does not work via the solvothermal method. Fig. 1(c) shows the XRD patterns of the (LMS@Ni)/C sample after the first charge and discharge process. The typical diffraction peaks belonging to Li_2MnSiO_4 cannot be observed, indicating that the crystal structure of Li_2MnSiO_4 changes into amorphous during

the cycling process. However, the peaks of metal Ni can still be observed, indicating that metal Ni is stable during the charge–discharge process.

SEM images of Li_2MnSiO_4, Li_2MnSiO_4/C and (LMS@Ni)/C are shown in Fig. 2. The particle size of the Li_2MnSiO_4/C is confined to 20–60 nm, much smaller and more uniform than that of the Li_2MnSiO_4 with size of 60–150 nm. This is attributed to the carbon coating, which separates the base particles and inhibits the growth of the particles during the calcinations process. The particle size of the (LMS@Ni)/C is about 20–50 nm, indicating that a small amount of Ni does not markedly affect the morphology of Li_2MnSiO_4/C.

Fig. 3 shows the TEM images of Li_2MnSiO_4/C and (LMS@Ni)/C. Before cycling, the lattice fringes and carbon coating layer can be observed clearly in Li_2MnSiO_4/C and (LMS@Ni)/C (Fig. 3(a) and Fig. 3(b), respectively). After the first cycle, the lattice fringes have become indistinct, as shown in Fig. 3(c) and Fig. 3(d). It indicates that the crystal structure of Li_2MnSiO_4 undergoes the process of amorphization, which is consistent with the XRD analysis.

Fig. 4 presents the TG data obtained for Li_2MnSiO_4/C. Water evaporation happens below 250 °C, carbon oxidation of $C + O_2 \rightarrow CO_2$ happens from 250 to 500 °C (the second mass decrease in TG), and weight addition caused by the transition of $Mn^{2+} \rightarrow Mn^{3+}$ happens from 500 to 1000 °C. As shown in Table 2, the content of carbon in Li_2MnSiO_4/C is 16.5 wt.%.

3.2. Electrochemical performance

Fig. 5 shows the cycling performance of Li_2MnSiO_4, Li_2MnSiO_4/C and (LMS@Ni)/C cathode materials, which was measured in the voltage range of 1.5–4.8 V at 0.05 C at 25 °C. The initial discharge capacity of Li_2MnSiO_4/C (259.9 mA h g^{-1}) is much higher than that of Li_2MnSiO_4 (15.7 mA h g^{-1}), which demonstrates that the carbon coating can effectively improve the discharge performance of Li_2MnSiO_4. However, the discharge capacity of Li_2MnSiO_4/C fades to 87.4 mA h g^{-1} after 20 cycles. The Ni-modified sample, (LMS@Ni)/C exhibits higher initial discharge capacity of 274.5 mA h g^{-1} and its discharge capacity remains 119.8 mA h g^{-1} after 20 cycles, demonstrating that the presence of Ni can improve the discharge performance of Li_2MnSiO_4/C. Fig. 6(a) and (b) shows the charge–discharge curves of Li_2MnSiO_4/C and (LMS@Ni)/C, respectively. There is no apparent voltage plateau in the curves, which may be caused by the low electrical conductivity and structural change of Li_2MnSiO_4 [27,32].

Table 3
The values of $a_{s,BET}$, A^* and C^* of Li_2MnSiO_4, Li_2MnSiO_4/C and (LMS@Ni)/C.

	$a_{s,BET}$ (m^2 g^{-1})	A (cm^2)	C (mol cm^{-3})
Li_2MnSiO_4	10.251	5.136	0.0196(6)
Li_2MnSiO_4/C	24.454	11.542	0.0196(8)
(LMS@Ni)/C	39.570	11.159	0.0197(0)

*A is the surface area of the cathode material, and C is the molar concentration of Li ions.

3.3. EIS measurements

Electrochemical impedance spectroscopy (EIS) measurements have been performed to investigate the effect of Ni on the Li ion migration dynamics. Fig. 7 shows the equivalent circuit and Nyquist plots of the three samples tested at 25 °C [33]. All of the Nyquist plots consist of a semicircle in the high to medium frequency region and an inclined line in the low frequency region. In the equivalent circuit, R_e represents the electrolyte resistance, corresponding to the intercept along the Z' axis, and R_{ct} represents the charge transfer resistance between the electrolyte and electrode material, corresponding to the diameter of the semicircle on the Z' axis. Z_W is the Warburg coefficient (the Li^+ diffusion in the bulk electrode), corresponding to the slope of the inclined line in the low frequency region. The lithium ion diffusion coefficient (D^+_{Li}) can be calculated as follows [34]:

$$D^+_{Li} = \frac{R^2T^2}{2A^2n^4F^4C^2\sigma^2} \quad (1)$$

In this equation, A is the surface area of the cathode material (listed in Table 3), n is the number of electrons per molecule involved in electron transfer (2 here), F is the Faraday constant (96,500 C mol^{-1}), C is the molar concentration of Li ions (listed in Table 3) [16], R is the gas constant (8.314 J K^{-1} mol^{-1}), T is room temperature (298 K), and σ is the slope of the fitting line.

Table 4 presents the parameters obtained from EIS analysis. R_{ct} value of Li_2MnSiO_4/C is much lower than that of Li_2MnSiO_4 before the first cycle, indicating that the carbon coating can improve the electronic conductivity of Li_2MnSiO_4. D^+_{Li} of Li_2MnSiO_4/C is 1.61×10^{-17} cm^2 s^{-1} before the first cycle, reducing to 1.28×10^{-19} cm^2 s^{-1} after the first cycle. However, D^+_{Li} of (LMS@Ni)/C is 2.96×10^{-17} cm^2 s^{-1} before the first cycle and 8.60×10^{-19} cm^2 s^{-1} after the first cycle, which is higher than that of Li_2MnSiO_4/C. R_{ct} value of (LMS@Ni)/C is 302.5 Ω, which is lower than that of Li_2MnSiO_4/C (338.0 Ω) after the first cycle. The above results indicate that the presence of Ni can improve the lithium ion diffusion coefficient as well as electronic conductivity of Li_2MnSiO_4/C cathode material.

4. Conclusions

Li_2MnSiO_4/C nanocomposite is prepared by the solvothermal method followed by carbon coating process. It is shown that Li_2MnSiO_4/C cathode material with smaller particles and higher electronic conductivity exhibits better electrochemical performance compared with the Li_2MnSiO_4 without carbon coating. The initial discharge capacity of Li_2MnSiO_4/C cathode is 259.9 mA h g^{-1}, which is much higher than that of Li_2MnSiO_4 (15.7 mA h g^{-1}). The presence of Ni improves the lithium ion diffusion coefficient as well as the electronic conductivity, resulting in the enhanced electrochemical performance of the (LMS@Ni)/C cathode material. The results indicate that it may be a strategy to improve the electrochemical performance for the cathode materials with poor conductivity by adding nano-metal.

Table 4
Impedance parameters of Li_2MnSiO_4, Li_2MnSiO_4/C and (LMS@Ni)/C cathodes before and after the first cycle.

	Before the first cycle			After the first cycle		
	Rct (Ω)	σ (Ω cm^2 $s^{-1/2}$)	D_{Li^+} (cm^2 s^{-1})	Rct (Ω)	σ (Ω cm^2 $s^{-1/2}$)	D_{Li^+} (cm^2 s^{-1})
Li_2MnSiO_4	97.40	205.57	5.11×10^{-18}	–	–	–
Li_2MnSiO_4/C	76.47	51.57	1.61×10^{-17}	338.0	577.72	1.28×10^{-19}
(LMS@Ni)/C	79.29	39.34	2.96×10^{-17}	302.5	230.75	8.60×10^{-19}

Acknowledgments

This project was supported by the National Natural Science Foundation of China (Grant No. 51372136), and Shenzhen Basic Research Project (Grant No. JCYJ20130402145002372).

References

[1] P.G. Bruce, B. Scrosati, J.M. Tarascon, Angew. Chem. Int. Ed. 47 (2008) 2930–2946.
[2] A. Magasinski, P. Dixon, B. Hertzberg, A. Kvit, J. Ayala, G. Yushin, Nat. Mater. 9 (2010) 353–358.
[3] D. Rangappa, K.D. Murukanahally, T. Tomai, A. Unemoto, I. Honma, Nano Lett. 12 (2012) 1146–1151.
[4] R. Dominko, J. Power Sources 184 (2008) 462–468.
[5] Z. Gong, Y. Yang, Energy Environ. Sci. 4 (2011) 3223–3242.
[6] Y. Wang, P. He, H. Zhou, Energy Environ. Sci. 4 (2011) 805–817.
[7] S.X. Zhao, H. Ding, Y.C. Wang, B.H. Li, C.W. Nan, J. Alloys Compd. 566 (2013) 206–211.
[8] M.R. Roberts, G. Vitins, J.R. Owen, J. Power Sources 179 (2008) 754–762.
[9] Y.H. Yin, M.S. Gao, J.L. Ding, Y.F. Liu, L.K. Shen, H.G. Pan, J. Alloys Compd. 509 (2011) 10161–10166.
[10] H. Yang, X.L. Wu, M.H. Cao, Y.G. Guo, J. Phys. Chem. C 113 (2009) 3345–3351.
[11] A. Nytén, A. Abouimrane, M. Armand, T. Gustafsson, J.O. Thomas, Electrochem. Commun. 7 (2005) 156–160.
[12] R. Dominko, M. Bele, A. Kokalj, M. Gaberscek, J. Jamnik, J. Power Sources 174 (2007) 457–461.
[13] C. Lyness, B. Delobel, A.R. Armstrong, P.G. Bruce, Chem. Commun. (2007) 4890–4892.
[14] C. Sirisopanaporn, C. Masquelier, P.G. Bruce, A.R. Armstrong, R. Dominko, J. Am. Chem. Soc. 133 (2010) 1263–1265.
[15] C.A.J. Fisher, N. Kuganathan, M.S. Islam, J. Mater. Chem. A. 1 (2013) 4207–4214.
[16] A. Kokalj, R. Dominko, G. Mali, A. Meden, M. Gaberscek, J. Jamnik, Chem. Mat. 19 (2007) 3633–3640.
[17] M.E. Arroyo deDompablo, U. Amador, J.M. Gallardo Amores, E. Morán, H. Ehrenberg, L. Dupont, R. Dominko, J. Power Sources 189 (2009) 638–642.
[18] T. Muraliganth, K.R. Stroukoff, A. Manthiram, Chem. Mat. 22 (2010) 5754–5761.
[19] V. Aravindan, K. Karthikeyan, K.S. Kang, W.S. Yoon, W.S. Kim, Y.S. Lee, J. Mater. Chem. 21 (2011) 2470–2475.
[20] D.M. Kempaiah, D. Rangappa, I. Honma, Chem. Commun. 48 (2012) 2698–2700.
[21] H. Duncan, A. Kondamreddy, P.H.J. Mercier, Y. Le Page, Y. Abu-Lebdeh, M. Couillard, P.S. Whitfield, I.J. Davidson, Chem. Mat. 23 (2011) 5446–5456.
[22] S. Zhang, Z. Lin, L. Ji, Y. Li, G. Xu, L. Xue, S. Li, Y. Lu, O. Toprakci, X. Zhang, J. Mater. Chem. 22 (2012) 14661–14666.
[23] Y.X. Li, Z.L. Gong, Y. Yang, J. Power Sources 174 (2007) 528–532.
[24] M. Kuezma, S. Devaraj, P. Balaya, J. Mater. Chem. 22 (2012) 21279–21284.
[25] W. Liu, Y. Xu, R. Yang, J. Alloys Compd. 480 (2009) L1–L4.
[26] S. Zhang, Y. Li, G. Xu, S. Li, Y. Lu, O. Toprakci, X. Zhang, J. Power Sources 213 (2012) 10–15.
[27] W. Liu, Y. Xu, R. Yang, Rare Met. 29 (2010) 511–514.
[28] V. Aravindan, K. Karthikeyan, S. Ravi, S. Amaresh, W.S. Kim, Y.S. Lee, J. Mater. Chem. 20 (2010) 7340–7343.
[29] M.S. Islam, R. Dominko, C. Masquelier, C. Sirisopanaporn, A.R. Armstrong, P.G. Bruce, J. Mater. Chem. 21 (2011) 9811–9818.
[30] J. Liu, H. Xu, X. Jiang, J. Yang, Y. Qian, J. Power Sources 231 (2013) 39–43.
[31] M.E. Arroyo deDompablo, R. Dominko, J.M. Gallardo Amores, L. Dupont, G. Mali, H. Ehrenberg, J. Jamnik, E. Morán, Chem. Mat. 20 (2008) 5574–5584.
[32] M. Świętosławski, M. Molenda, K. Furczoń, R. Dziembaj, J. Power Sources 244 (2013) 510–514.
[33] S. Liu, J. Xu, D. Li, Y. Hu, X. Liu, K. Xie, J. Power Sources 232 (2013) 258–263.
[34] X. Wang, H. Hao, J. Liu, T. Huang, A. Yu, Electrochim. Acta 56 (2011) 4065–4069.